CHEMISTRY
A EUROPEAN JOURNAL

FULL PAPER

DOI: 10.1002/chem.201301990

In Silico Design of Heteroaromatic Half-Sandwich Rh^I Catalysts for Acetylene [2+2+2] Cyclotrimerization: Evidence of a Reverse Indenyl Effect

Laura Orian,*[a] Lando P. Wolters,[b] and F. Matthias Bickelhaupt*[b, c]

Abstract: A mechanistic density functional theory study of acetylene [2+2+2] cyclotrimerization to benzene catalyzed by Rh^I half metallocenes is presented. The catalyst fragment contains a heteroaromatic ligand, that is, the 1,2-azaborolyl (Ab) or the 3a,7a-azaborindenyl (Abi) anions, which are isostructural and isoelectronic to the hydrocarbon cyclopentadienyl (Cp) and indenyl (Ind) anions, respectively, but differ from the last ones on having two adjacent carbon atoms replaced with a boron and a nitrogen atom. The better performance of either the classic hydrocarbon or the heteroaromatic catalysts is found to depend on the different mechanistic paths that can be envisioned for the process. The present analyses uncover and explain general structure–reactivity relationships that may serve as rational design principles. In particular, we provide evidence of a reverse indenyl effect.

Keywords: activation strain analysis · catalyst design · cyclotrimerization · density functional calculations · indenyl effect · rhodium

Introduction

In cyclopentadienyl (Scheme 1: Cp) and indenyl (Scheme 1: Ind) anions, the replacement of one of the C–C bonds of the cyclopentadienyl moiety by an isoelectronic B–N bond leads to interesting heteroaromatic ligands, that is, 1,2-azaborolyl (Scheme 1: Ab) and 3a,7a-azaborindenyl (Scheme 1: Abi) anions, which, after the pioneering studies of Schmid,[1] have been more recently synthesized by Fu[2] and Ashe.[3] Zr^{IV} complexes of Ab ($R = C_6H_5$, $R' = CH_3CH_2$) and Abi were found to display a higher activity as Ziegler–Natta catalysts for the polymerization of olefins than the analogous Cp and Ind derivatives.[3c] Schmid reported also that the AbCo fragment is an excellent catalyst for alkyne cyclotrimerizations.[1b]

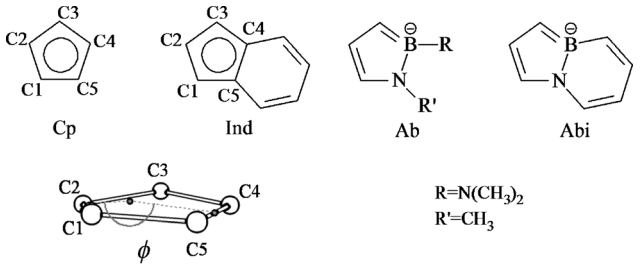

Scheme 1. Cyclopentadienyl (Cp), indenyl (Ind), 1,2-azaborolyl (Ab) and 3a,7a-azaborindenyl (Abi) anions.

In contrast to the ubiquitous Cp, both substituted Cp and heteroaromatic Cp analogues are less employed in organometallic complexes, mainly due to synthetic difficulties, although the presence of substituents in the Cp ring might indeed modify the electron density at the coordinated metal center and allow a fine tuning of its reactivity. The Ab ligand is an interesting example, in which the boron and nitrogen atoms break the symmetry without altering the total number of π electrons and, at the same time, serve as points of attachment for substituents that can be used to adjust the electronic environment of the coordinated metal.

In this study, we have modeled half-sandwich Rh^I complexes of ligands Ab and Abi with the aim of investigating 1) if and how the bonding mode and the reactivity of the metal changes when compared to the parent complexes containing the hydrocarbon Cp and Ind ligands and 2) if there is the possibility of tuning the reactivity of the metal by introducing different substituents at boron and at nitrogen in the Ab ligand. In particular, we have employed the AbRh and AbiRh fragments in silico as catalysts in the [2+2+2] cyclotrimerization of acetylene to benzene, a reaction of paramount importance in chemistry.[4] In fact, metal-catalyzed cyclotrimerizations of alkynes and more, in general, unsaturated molecules represent a convenient and a versatile synthetic route to a variety of substituted benzenes, heterocyclic and polycyclic compounds useful in chemical and

[a] Dr. L. Orian
Dipartimento di Scienze Chimiche
Università degli Studi di Padova
Via Marzolo 1, 35129 Padova (Italy)
E-mail: laura.orian@unipd.it

[b] L. P. Wolters, Prof. Dr. F. M. Bickelhaupt
Department of Theoretical Chemistry and
Amsterdam Center for Multiscale Modeling
VU University Amsterdam, De Boelelaan 1083
1081 HV Amsterdam (The Netherlands)
E-mail: f.m.bickelhaupt@vu.nl

[c] Prof. Dr. F. M. Bickelhaupt
Radboud University Nijmegen, Institute for Molecules and Materials
Heyendaalseweg 135, 6525 AJ Nijmegen (The Netherlands)

Supporting information for this article is available on the WWW under http://dx.doi.org/10.1002/chem.201301990.

pharmaceutical industry and research. A comparison is systematically made with Rh^I catalysts containing the classic Cp and Ind ligands, the activity of which has been studied experimentally[5] as well as in silico.[6]

The replacement of two C atoms with B and N, which drastically lowers the symmetry near the metal center, first implies significant geometric distortions as quantified in a preceding study.[7] In Cp and Ind complexes the metal bonding mode is quantitatively described by defining the slippage parameter Δ [Eq. (1)], in which M−C4 and M−C5 are the longest distances between M and two adjacent C atoms of the Cp ring and M−C3 and M−C1 are the distances between M and the C atoms adjacent to C4 and C5, respectively (the C atoms are labeled in the anions of Scheme 1; in indenyl complexes C4 and C5 correspond to the hinge carbon atoms).[7,8]

$$\Delta = 1/2[(M{-}C4 + M{-}C5){-}(M{-}C1 + M{-}C3)] \quad (1)$$

In Ind, but also in Cp complexes, the ground-state hapticity of the metal is not symmetric with respect to the centroid Q of the five-membered ring; that is, the five metal–carbon distances are not equal. Thus, in Cp and especially in Ind derivatives the bonding mode is better described as $\eta^3+\eta^2$, a structural peculiarity mainly related to the metal–ligand bond strength.[9] In Cp and Ind complexes, the metal slippage is often accompanied also by folding of the Cp ring, here quantified by the angle ϕ defined by the rays connecting the midpoint of the bond C4−C5 (or B−N in the heteroaromatic ligands) to the midpoint of the distance C1−C3 and this latter with the atom C2 (Scheme 1). In Ab and Abi complexes, the slippage is always more pronounced than in the analogous Cp and Ind compounds; this in particular is more evident when electron-rich metals are coordinated.[1e–i] For example, when the crystal structures of (η^4-cycloocta-1,5-diene)(η^5-cyclopentadienyl)rhodium ([CpRh(cod)]),[10a] (η^4-cycloocta-1,5-diene)(η^3-indenyl)rhodium ([IndRh(cod)])[10b] and (η^4-cycloocta-1,5-diene)(η^5-1-*tert*-butyl-2-diisopropylamino-1,2-azaborolyl)rhodium are compared,[10c] the distance Rh−Q, the slippage parameter Δ[11] and the folding angle of the five-membered ring are 1.91, 1.93 and 1.96 Å; 0.047, 0.15 and 0.27 Å; and 3, 9 and 12°, respectively. Does the enhanced slippage in presence of the heteroaromatic ligand imply a greater reactivity? The fluxionality of the metal–ring bonding mode is typically associated with reactivity enhancement, but the connection between the structural properties of a catalyst and its activity is not so straightforward.

In this study, we investigate if the mechanistic paths envisioned for CpRh- and IndRh-catalyzed [2+2+2] acetylene cyclotrimerization, which have been extensively described by us in a previous paper,[6] are still valid when AbRh and AbiRh fragments are employed and compare the activity of the aromatic and heteroaromatic catalysts, for which experimental data are still scarce. Novel insights on the structure–reactivity relationship of these Rh^I half-metallocenes emerge from our analysis. One of the highlights that emerges is a hitherto unknown reverse indenyl effect, that is, a reduced (and not increased) reactivity in an oxidative coupling step in the case of more pronounced slippage of the aromatic ligand.

Computational Methodology

All density functional theory (DFT)[12] calculations were done with the Amsterdam Density Functional (ADF) program.[13,14] Calculations were done with scalar relativistic effects accounted for using the zeroth-order regular approximation (ZORA).[15] The BLYP[16] density functional was used, in combination with the TZ2P basis set for all elements. The TZ2P basis set was a large uncontracted set of Slater-type orbitals (STOs) of triple-ζ quality and was augmented with two sets of polarization functions on each atom: 2p and 3d in the case of H, 3d and 4f in the case of C and N, and 5p and 4f in the case of Rh. An auxiliary set of s, p, d, f and g STOs was used to fit the molecular density and to represent the Coulomb and exchange potentials accurately in each SCF cycle.[13] The frozen-core approximation was employed: up to 1s for C and N and up to 3d for Rh. The electronic structures of the intermediates and transition-state geometries were analyzed in terms of the quantitative molecular orbital (MO) model contained in Kohn–Sham DFT.[17] Recently, it has been shown that our approach is in satisfactory agreement with high-level ab initio calculations for oxidative addition reactions of the C−H,[18] C−C,[19] C−F,[20] and C−Cl[21] bonds to palladium.

Equilibrium and transition-state geometries were fully optimized by using analytical gradient techniques. All structures were verified by frequency calculations: for minima all normal modes have real frequencies, whereas transition states have one normal mode with an imaginary frequency. The character of the normal mode associated with the imaginary frequency was analyzed to ensure that the correct transition state was found. The experimental benchmark for the computed structures is described in previous papers by us.[6,22] Structural and energy data of CpRh and IndRh catalysis were taken and used for comparison from reference [6].

Solvent effects in toluene and acetonitrile have been estimated using the conductor-like screening model (COSMO),[23] as implemented in the ADF program.[14] We used a solvent-excluding surface with an effective radius of 2.53 Å for toluene and 1.967 Å for acetonitrile, derived from the macroscopic densities, molecular masses, and a relative dielectric constants of 0.866 and 0.786 $g\,mL^{-1}$; 92.14 and 41.05 $g\,mol^{-1}$; and 2.379 and 36.64, respectively. The empirical parameter in the scaling function in the COSMO equation was chosen to be 0.0. The radii of the atoms were taken to be MM3 radii,[24] divided by 1.2, giving 1.350 Å for H, 1.700 Å for C, 1.608 Å for N, 1.517 Å for O, and 1.950 Å for Rh (see also reference [25]).

To arrive at a better understanding of how barriers of key elementary reaction steps depend on the nature of the catalytically active complex, we have carried out activation strain analyses. The activation strain model is a fragment-based approach to understanding chemical reactions and the associated barriers.[17] The starting point is the two separate reactants, which approach from infinity and begin to interact and deform each other. In this model, the activation energy $\Delta E^{\neq}$ of the transition state (TS) is decomposed into the strain energy $\Delta E^{\neq}_{strain}$ and the interaction energy $\Delta E^{\neq}_{int}$ [Eq. (2)]

$$\Delta E^{\neq} = \Delta E^{\neq}_{strain} + \Delta E^{\neq}_{int} \quad (2)$$

The activation strain $\Delta E^{\neq}_{strain}$ is the energy associated with deforming the reactants from their equilibrium geometry into the geometry they acquire in the activated complex. It can be divided into a contribution stemming from each of the reactants, for example, catalyst and substrate strain in the case of catalytic bond activation. The TS interaction $\Delta E^{\neq}_{int}$ is the actual interaction energy between the deformed reactants in the transition state. It can be further analyzed in the framework of the Kohn–Sham molecular orbital (MO) model using a quantitative decomposition

of the bond into electrostatic interaction, Pauli repulsion (or exchange repulsion or overlap repulsion), and (attractive) orbital interactions.[17d] Recently, Fernandez et al.[26] proposed an extension to the activation strain model for unimolecular reaction steps in which chemically meaningful fragments can be discerned. This situation is encountered in key steps in the present study, that is, when a five-membered rhodacycle [(L)Rh-(C_4H_4)] is formed from a bis-acetylene precursor [(L)Rh(C_2H_2)] and when an LRh fragment is eliminated from a [(L)Rh(C_6H_6)] seven-membered rhodacycle furnishing a [(L)Rh(benzene)] complex. Thus, the activation barrier is now given as the change, upon going from the reactant to the TS, in strain within the two fragments plus the change, upon going from the reactant to the TS, in the interaction between these two fragments [Eq. (3)]

$$\Delta E^{\neq} = \Delta\Delta E^{\neq}_{\text{strain}} + \Delta\Delta E^{\neq}_{\text{int}} \tag{3}$$

The TOFs (turn-over frequencies) of the catalytic cycles have been calculated employing the energetic span model. Based on an idea of Amatore and Jutand,[27] subsequently developed and implemented by Kozuch and Shaik,[28] this model relies on three assumptions, that is, 1) transition-state theory (TST) is valid; 2) a steady-state regime subsists, and 3) the relaxation of the intermediates is fast. The equation derived for TOF is given by Equation (4), in which $\Delta G_r$is the reaction free energy, TS_i and I_i are the Gibbs energies of the i-th transition state and j-th intermediate, respectively, and $\delta G_r^{i,j} = \Delta G$ if $i > j$ or 0 if $i \leq j$.

$$\text{TOF} = \frac{k_B T}{h} \frac{e^{-\Delta G_r/RT} - 1}{\sum_{i,j=1}^{N} e^{\left(TS_i - I_j - \delta G'_{ij}\right)/RT}} \tag{4}$$

In the case of exothermic reactions and when a single term of the summation dominates in the denominator, Equation (4) can be simplified as Equation (5), in which δE, called the energetic span, is given by Equation (6).

$$\text{TOF} = \frac{k_B T}{h} e^{-\delta E/\text{RT}} \tag{5}$$

$$\begin{aligned} \delta E &= TS_{\text{TDTS}} - I_{\text{TDI}} \text{ if TDTS appears after TDI} \\ &= TS_{\text{TDTS}} - I_{\text{TDI}} + \Delta G_r \text{ if TDTS appears before TDI} \end{aligned} \tag{6}$$

TDTS and TDI are the TOF-determining transition state and the TOF-determining intermediate, that is, the transition state and the intermediate that maximize the energetic span within the constraints of Equation (6). TDTS and TDI can be identified using the degree of TOF control, defined as Equation (7)

$$X_{\text{TOF},i} = \left| \frac{1}{\text{TOF}} \frac{\partial \text{TOF}}{\partial E_i} \right| \tag{7}$$

in which E_i can be a transition state or an intermediate Gibbs energy. The bigger $X_{\text{TOF}I}$, the higher the influence on the kinetics of the the corresponding state. Combining Equations (4) and (7), we can derive Equation (8).

$$\begin{aligned} X_{\text{TOF,TS}_i} &= \frac{\sum_j e^{\left(TS_i - I_j - \delta G'_{ij}\right)/RT}}{\sum_{ij} e^{\left(TS_i - I_j - \delta G'_{ij}\right)/RT}} \\ X_{\text{TOF,I}_j} &= \frac{\sum_i e^{\left(TS_i - I_j - \delta G'_{ij}\right)/RT}}{\sum_{ij} e^{\left(TS_i - I_j - \delta G'_{ij}\right)/RT}} \end{aligned} \tag{8}$$

Although TST and thus the energy span model require Gibbs energies, E can be used if the determining elementary reactions have the same molecularity, but, most of all, if one is interested in relative TOFs, like in our case, which can be a reliable quantitative result due to error compensation. Very recently we have demonstrated for analogous Rh^I-catalyzed [2+2+2] acetylene cyclotrimerizations that indeed the energy profiles and corresponding TOF ratios do not change significantly when using energies E instead of Gibbs free energies G.[29] Therefore, in the present work, we use and discuss energies E.

Results and Discussion

Scheme 2 shows the possible mechanistic pathways of LRh-catalyzed acetylene [2+2+2] cyclotrimerization;[6] the legend for L is shown in the scheme. For clarity, we have redefined compounds with L = **a**–**d** introducing the abbreviations of the aromatic/heteroaromatic ligands shown in Scheme 1, that is, L = Cp (**a**), Ind (**b**), Ab (**c**), and Abi (**d**).

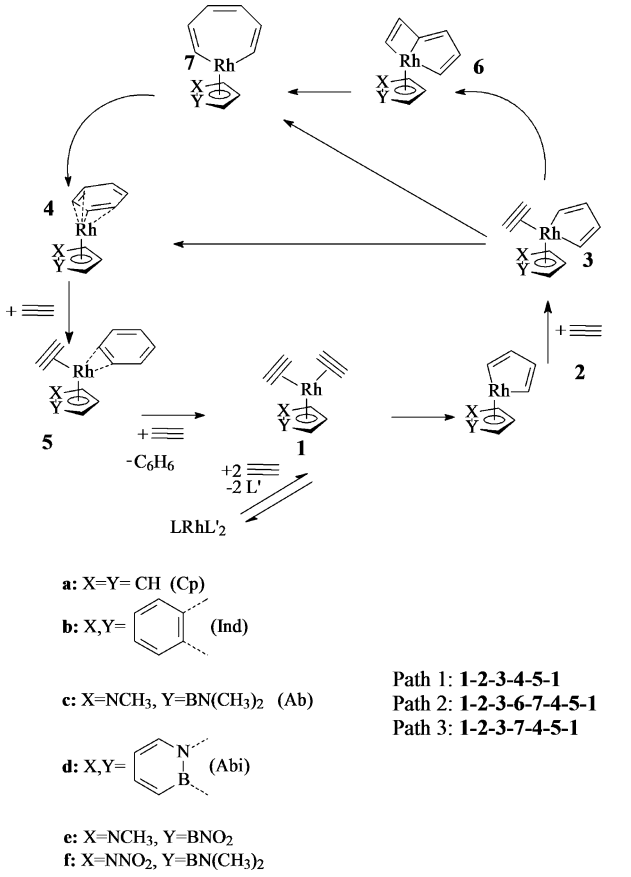

Scheme 2. Possible mechanistic paths of LRh catalyzed acetylene [2+2+2] cyclotrimerization; L = **a**-**f**; L′ indicates an ancillary ligand of the catalyst precursor.

At the beginning of the catalytic cycle the ancillary ligands L′ of the catalyst precursor, typically L′ = C_2H_4, CO, PH_3 or L′$_2$ = 1,5-cyclooctadiene, are replaced by two acetylene molecules and complex **1** forms. By oxidative coupling, complex **1** converts into the unsaturated 16-electron rhodacycle **2**. The facile coordination of a third acetylene molecule (**3**), and its subsequent addition to the π-electron system of the rhodacycle, leads to the formation of an inter-

mediate (**4**), which is characterized by a six-membered arene ring coordinated to the metal in η^4 fashion. The release of benzene occurs by stepwise addition of two acetylene molecules, passing through the intermediate **5**, and is accompanied by the regeneration of the catalyst. Alternatively the bicyclic complex **6** can form from **3** and evolve to the heptacyclic intermediate **7**, which, by reductive elimination, is converted into **4**. Complex **7** can be formed also from **3** by direct insertion of the coordinated acetylene into the Rh–C_α bond (Schore's mechanism).[30] In reference [6], we have described the path **1**→**2**→**3**→**4**→**5**→**1** (Path 1) for CpRh- and IndRh-catalyzed acetylene [2+2+2] cyclotrimerization. This path closely resembles the mechanism postulated by Albright et al.[31] for the CpCo-catalyzed process. Bicyclic and heptacyclic intermediates, analogous to **6** and **7**, have been postulated for [CpRuCl]-catalyzed acetylene [2+2+2] cyclotrimerization,[32] by us for CpRh-catalyzed acetylene/acetonitrile cyclocotrimerization to 2-methylpyridine,[6] and very recently in novel mechanisms proposed for CpRh(CO)- and IndRh(CO)-catalyzed acetylene [2+2+2] cyclotrimerization to explain the experimentally observed "indenyl effect".[29]

We started our investigation exploring Path 1, that is, following the classic CpCo-like mechanism also for Ab/AbiRh catalysis. In **Ab-1**, the two acetylene molecules are tilted off from the plane parallel to the aromatic ligand and suitably oriented for the formation of the bent rhodacycle **Ab-2** (Figure 1). In the transition-state geometry **Ab-TS12**, they approach one another and the interatomic C–C and Rh–C distances become much closer to the corresponding values of the product. Despite the fact that **Ab-1** adopts a more favorable, that is, product-like geometry than **Cp-1** in which the acetylenes lie parallel to each other and to the ring plane,[6] the activation energy is higher for the former than for the latter, that is, 17.6 versus 12.5 kcal mol^{-1}. This is in contrast with what has been predicted for the same elementary reaction in the case of cobaltacycle formation, which has an activation enthalpy of 10.7 versus 11.7 kcal mol^{-1} when AbCo and CpCo fragments, respectively (structurally very similar to AbRh and CpRh), are used.[7] In order to gain insight into the remarkable difference in the activation energy of the elementary step **1**→**2** when the Ab ligand is used instead of the parent Cp ligand an activation strain analysis has been carried out on **Cp-1** and **Ab-1** as well as on **Cp-TS12** and **Ab-TS12**. The results are shown in Table 1.

The fragments are two free acetylene molecules (the reference energy is twice the energy of an isolated acetylene) and the LRh (L = Ab, Cp) moiety and all the values refer to their energies. Both in the reactant and TS, the strain is less destabilizing and the interaction less attractive for L = Ab than for L = Cp. However, while the strain contributions $\Delta\Delta E^{\neq}_{strain}$ to the activation energy $\Delta E^{\neq}$ are comparable, a 4.3 kcal mol^{-1} more stabilizing contribution of interaction $\Delta\Delta E^{\neq}_{int}$ is calculated in the latter case. This entirely accounts for the difference in the calculated barriers. The step **Ab-1**→**Ab-TS12**→**Ab-2** and **Cp-1**→**Cp-TS12**→**Cp-2** is accompanied by a change in slippage Δ and folding angle ϕ [see Equation (1) and Scheme 1). In particular, Δ varies from 0.55 to 0.20 and to 0.24 in the former and from 0.06 to 0.10 and to 0.13 Å in the latter case; the corresponding values of ϕ are 16.4, 10.7 and 12.6, and 3.6, −1.1 and −5.7, respectively. Thus, in the presence of the heteroaromatic ligand, intermediates and transition state show more pronounced η^3 coordination and folding, and a stronger hapticity variation of opposite sign accompanies the formation of the metallacycle. In fact, Rh moves closer to [N–B$^-$] during this **1**→**2** step, because upon oxidation it experiences a stronger pull by the negative B$^-$. Another important difference is the release of 23.3 kcal mol^{-1} when **Ab-2** forms; in the case of **Cp-2** only 18.3 kcal mol^{-1} are released.

Table 1. Activation strain analysis of **Cp/Ind/Ab/Abi-1** and **Cp/Ind/Ab/Abi-TS12**.[a]

	$2(C_2H_2)$	$\Delta\Delta E^{\neq}_{strain}$ LRh	Total	$\Delta\Delta E^{\neq}_{int}$	$\Delta E^{\neq}$[b]
Cp-1/Cp-TS12	31.9	2.3	34.2	−21.7	12.5
Ab-1/Ab-TS12	33.5	1.5	35.0	−17.4	17.6
Ind-1/Ind-TS12	36.3	2.7	39.0	−23.9	15.1
Abi-1/Abi-TS12	34.5	2.3	36.8	−20.6	16.2

[a] Computed at ZORA-BLYP/TZ2P; all values are in kcal mol^{-1}. [b] Activation energy: $\Delta E^{\neq} = \Delta\Delta E^{\neq}_{strain} + \Delta\Delta E^{\neq}_{int}$.

The coordination of the third acetylene molecule occurs very easily (formation of **Ab-3**) and an activation energy of 9.0 kcal mol^{-1} is required to convert this adduct into **Ab-4**, which lies 63.5 kcal mol^{-1} below its precursor. The activation energy computed for the corresponding step **Cp-3**→**Cp-4** is lower (4.7 kcal mol^{-1}). Finally, the displacement of benzene from **Ab-4** is stepwise and occurs with negligible or zero energy barriers, accompanied by the release of 15.0 and 17.8 kcal mol^{-1}, respectively. The energy profile of this mechanism is shown in Figure 2 (top), in which CpRh and IndRh energetics[6] are included for comparison.

An analogous mechanism may be postulated for the AbiRh-catalyzed process; the intermediates and transition states are shown in Figure 3.

The activation energies for the formation of the metallacycle **Abi-2** and of the intermediate **Abi-4**, 16.2 and 7.7 kcal mol^{-1} respectively, are slightly lower than those computed for AbRh catalysis, but still higher than those previously reported by us for CpRh and IndRh (Figure 2, top). It is also evident that the largest difference in the energetics between the Ab/Abi- and Cp/Ind-catalyzed processes occurs in the final part of the catalytic cycle, that is, in the step **4**→**5**. In particular, the intermediates **Ab/Abi-4** and **Ab/Abi-5** are more stabilized than the corresponding **Cp/Ind-4** and **Cp/Ind-5**. In the case of complexes **4**, this can be ascribed to the fact that in **Ab/Abi-4** the benzene ligand is already planar (Figure 1 and 3), whereas in **Cp/Ind-4** it is bent.[10] Consequently, **Ab/Abi-4** already benefits from the energetically favorable intact aromatic system, whereas **Cp/Ind-4** does not.

Solvent effects have been investigated in AbRh catalysis using the COSMO continuum model for the dielectric environment. Acetonitrile and toluene have been considered for their significantly different polarity. It is worth noting that for these reactions no solvents are generally used, but the

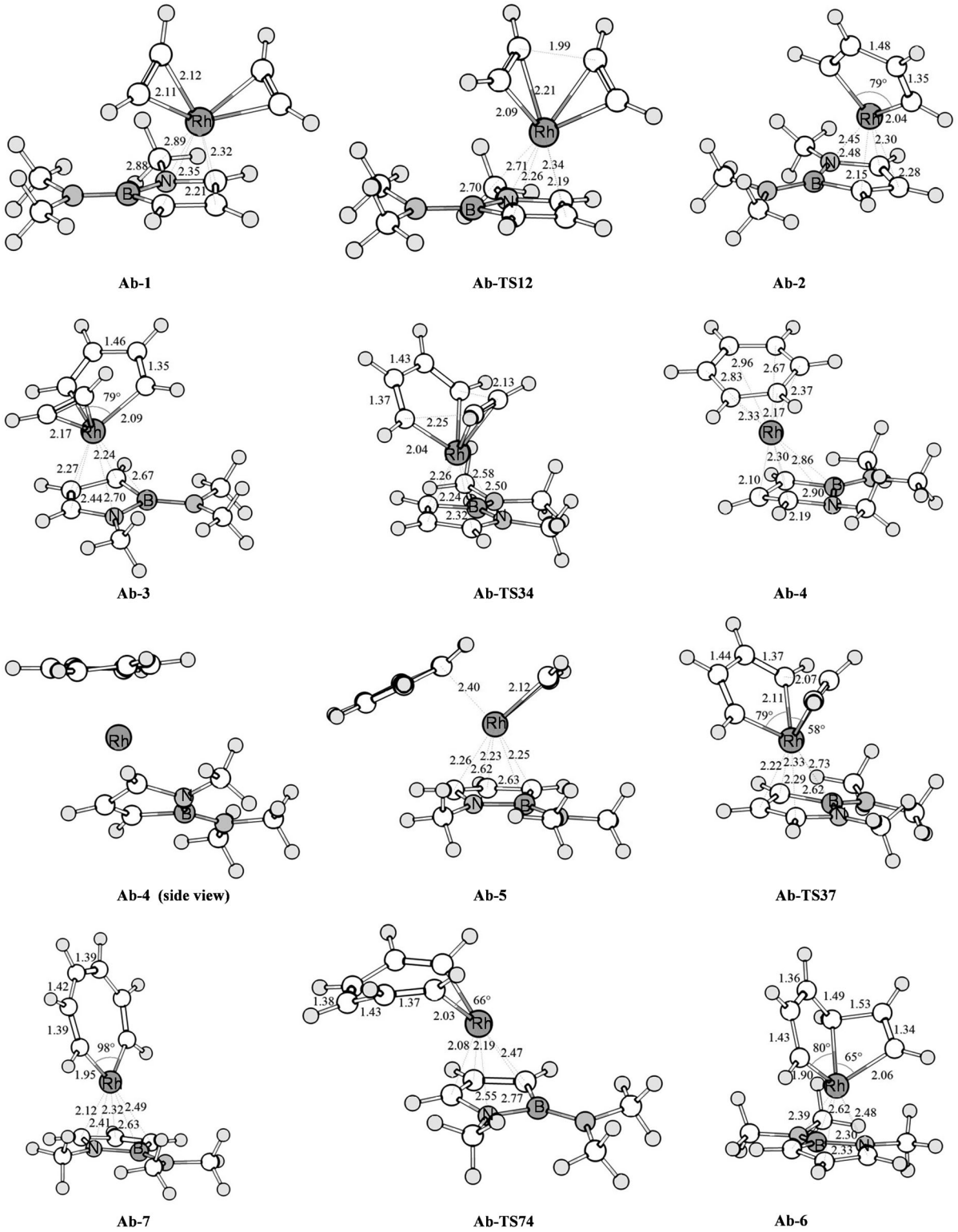

Figure 1. Molecular structures with relevant interatomic distances [Å] and angles [°] of the intermediates and transition states of AbRh-catalyzed acetylene [2+2+2] cyclotrimerization.

product is itself the reaction's solvent.[5] The presence of a dielectric medium has a stabilizing effect on the intermediates and transition states that increases with the polarity of the solvent (Figure 2, bottom), without essentially altering the energy profile. This activation energy of the step **Ab-1**→**Ab-2** slightly decreases when going from vacuum to toluene and acetonitrile. The overall effect due to the solvent can be quantified through the ratio of TOF(solv):TOF(g) at 373 K

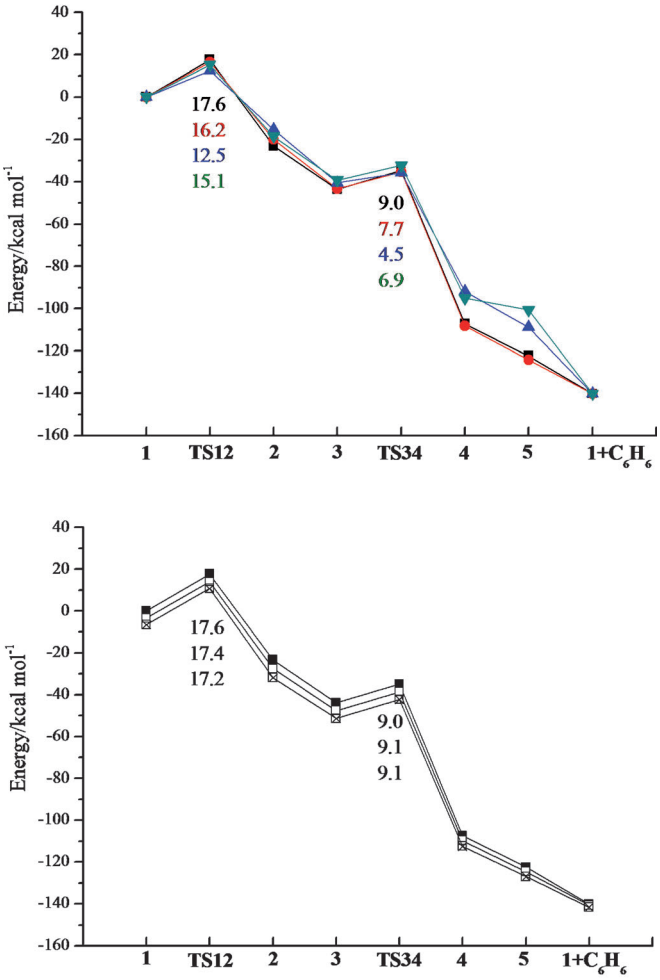

Figure 2. Top: Path 1: energy profile of AbRh (black squares)-, AbiRh (red circles)-, CpRh (blue triangles)-, and IndRh (green triangles)-catalyzed acetylene [2+2+2] cyclotrimerization; activation energies (in kcal mol^{-1}) are shown. Bottom: Path 1: energy profile of AbRh catalyzed acetylene [2+2+2] cyclotrimerization in vacuo (filled squares), in toluene (empty squares) and in acetonitrile (squares with cross); energy values are relative to the free reactants in vacuo; activation energies (in kcal mol^{-1}) are shown.

which amounts to 1.3 and 1.7 at 373 K for toluene and acetonitrile, respectively.

The ratios of the turnover frequencies of the four catalytic cycles of Figure 2 (top) have also been calculated for a quantitative comparison; a temperature of 373 K has been chosen. On the basis of the TOF ratios, reported in Table 2, this trend of catalytic efficiency emerges: CpRh > IndRh > AbiRh > AbRh. We can thus conclude that 1) the heteroaromatic catalysts are worse than their parent hydrocarbon analogues in catalyzing the acetylene [2+2+2] cyclotrimerization; and 2) the indenyl effect, which is not operative in this mechanism when comparing CpRh and IndRh catalysts, is revealed, although moderately, when the heteroaromatic indenyl AbiRh fragment is used rather than the heteroaromatic AbRh. To gain insight on this result, and more in general to inspect the structural changes along the catalytic cycle, the distances Rh–C4 and Rh–C5, and Rh–N and Rh–B have been plotted for Ab/AbiRh and Cp/IndRh intermediates and transition states (Figure 4).

Table 2. TOF ratios calculated at 373 K for different mechanistic paths.

	Path 1	Path 3
CpRh	975	1
IndRh	30	–
AbRh	1	2100
AbiRh	7	10100

In AbRh and AbiRh catalyzed cycles, intermediates and transition states are characterized by a pronounced allylic coordination. In addition, the distances Rh–N and Rh–B vary up to 0.5 Å, suggesting that strong hapticity variations occur during these cycles. Instead, in the CpRh-catalyzed cycle, the hapticity is closer to η^5 and the distances Rh–C4 and Rh–C5 vary by the same amount (less than 0.2 Å) due to the nearly C_s symmetry. Finally, in the IndRh-catalyzed reaction, the hapticity of intermediates and transition states can be better described as $\eta^3+\eta^2$ and hapticity variations are less pronounced than in Ab/AbiRh, but more pronounced than in CpRh case. Thus, in the most efficient cycle there is little hapticity variation and the coordination of the metal remains closer to almost η^5. This confirms what we have previously observed when comparing the catalytic activity of IndRh and CpRh for the acetylene [2+2+2] cyclotrimerization: the higher the distortion from η^5 coordination and the hapticity variations during the cycle, the worse the TOF.[6,29] This finding contrasts with the well-known indenyl effect in which more facile (and thus more pronounced) slippage leads to a lower barrier. The indenyl effect, first described for ligand substitution reactions by Basolo,[33] has been reported also for catalytic processes and in particular for the studied cyclotrimerization.[5] We designate the phenomenon, that more slippage goes with a higher barrier, the "reverse indenyl effect".[34]

In order to elucidate the differences in the catalytic activity of the four fragments along this path, we have carried out an activation strain analysis on **Ab-1** and **Abi-1** as well as on **Ab-TS12** and **Abi-TS12** and on the corresponding couples of Cp and Ind complexes and the results are reported in Table 1. In the case of Ab and Abi, $\Delta\Delta E^{\neq}_{strain}$ values are rather similar, but the larger $\Delta\Delta E^{\neq}_{int}$ in the latter explains the lower activation energy when Abi is used. Instead it is the larger $\Delta\Delta E^{\neq}_{strain}$ calculated in the case of Ind, which is not entirely compensated by the $\Delta\Delta E^{\neq}_{int}$ term, that determines the higher energy barrier when Cp is replaced by Ind in step **1**→**2**. Interestingly, the lower activation energy calculated for AbiRh than AbRh corresponds to less slippage in the former, consistently with reverse indenyl effect.

The effects of different substituents at boron and at nitrogen in Ab ligand have been explored by investigating the rate (or TOF)-determining step, that is, the step connecting the TOF-determining intermediate and the TOF-determining transition state, which are in this case consecutive, identified along Path 1 as the oxidative coupling **1**→**2**. Six differ-

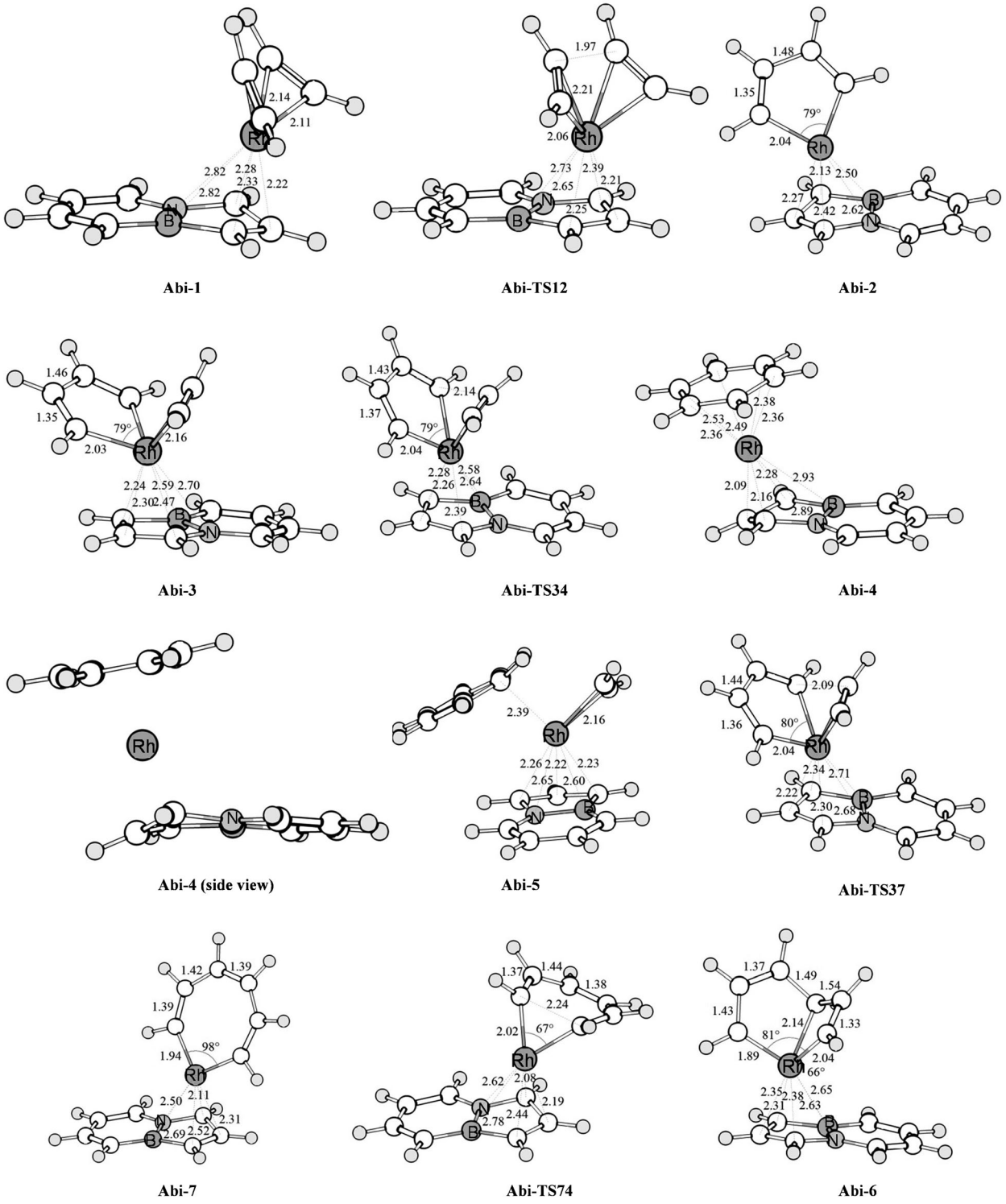

Figure 3. Molecular structures with relevant interatomic distances and angles of the intermediates and transition states of AbiRh-catalyzed acetylene [2+2+2] cyclotrimerization.

ent substituents at boron (R = F, Cl, Br, I, C_6H_5, NO_2) have been used, while keeping the substituent at nitrogen R′ = CH_3, as in our model Ab ligand (Scheme 1) and, conversely, six different substituents at nitrogen (R′ = F, Cl, Br, I, C_6H_5, NO_2) have been used, while keeping the substituent at boron R = $N(CH_3)_2$. The calculated activation and reaction energies are reported in Table 3, in which the values calculated for Cp, Ind, Abi, and Ab are also included for comparison. Varying the substituent R′ at N in Ab causes the activation energy to increase in all reported cases. In contrast,

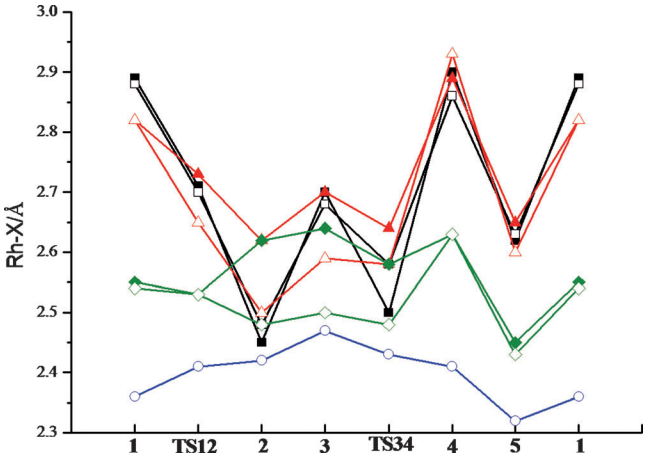

Figure 4. Variation of bond lengths Rh–B (empty squares and triangles), Rh–N (filled squares and triangles), Rh–C4 (empty circles and diamonds) and Rh–C5 (filled circles and diamonds) in the intermediates and transition states of AbRh (black), AbiRh (red), CpRh (blue) and IndRh (green) catalyzed acetylene [2+2+2] cyclotrimerization.

Table 3. Effects of different substituents at B and N on the activation energy and the reaction energy of step **1**→**2** of Path 1.[a]

		$\Delta E^{\neq}$ (**1**→**2**)	ΔE
Cp		12.5	−18.3
Ind		15.1	−21.8
Ab		17.6	−23.3
Abi		16.2	−20.6
R′=CH_3	R=F	20.0	−22.1
R′=CH_3	R=Cl	15.9	−22.3
R′=CH_3	R=Br	15.7	−22.4
R′=CH_3	R=I	15.4	−22.5
R′=CH_3	R=C_6H_5	15.4	−23.8
R′=CH_3	R=NO_2	14.4[b]	−21.7[b]
R=$N(CH_3)_2$	R′=F	20.8	−20.5
R=$N(CH_3)_2$	R′=Cl	19.6	−22.0
R=$N(CH_3)_2$	R′=Br	20.0	−23.8
R=$N(CH_3)_2$	R′=I	18.8	−24.7
R=$N(CH_3)_2$	R′=C_6H_5	18.4	−22.7
R=$N(CH_3)_2$	R′=NO_2	23.0[c]	−17.9[c]

[a] Computed at ZORA-BLYP/TZ2P; all values are in kcal mol^{-1}. [b] These values refers to the reaction **e-1**→**e-2**. [c] These values refers to the reaction **f-1**→**f-2**.

all the tested substituents R at B induce a decrease of the activation energy and thus represent an improvement with respect to Ab, with the exception of R=F. The most striking difference is the effect of NO_2 in both positions; when R=NO_2 (L=**e**) and when R′=NO_2 (L=**f**), we predict the lowest and the highest activation energy for the oxidative coupling **1**→**2**, that is, 14.4 and 23.0 kcal mol^{-1}, respectively. Importantly, the catalyst **e** has a lower activation energy for the step **1**→**2** than IndRh, which has been experimentally tested and has shown a good catalytic activity in alkyne cyclotrimerizations.[5] Figure 5 shows the structures **e-1**, **e-TS12**, **e-2** and **f-1**, **f-TS12**, **f-2**. Along **1**→**TS12**→**2**, the slippage parameter Δ [see Eq. (1)] and folding angle ϕ amount, in **e-1**, **e-TS12**, **e-2**, to 0.32, 0.25, and 0.0009 Å, and 8.8, 5.3, and 6.4° and, in **f-1**, **f-TS12**, **f-2**, to 0.63, 0.44 and 0.32 Å, and 22.2, 14.3 and 12.8°, respectively. This reconfirms that 1) upon oxidation the metal center tends to move closer to the heteroatoms, attracted by the negative boron, and 2) the reaction **f-1**→**f-2**, in which the distortion from η^5 coordination is more pronounced, has a higher activation energy (reverse indenyl effect).

We have investigated the existence of alternative mechanistic paths in presence of the heteroaromatic catalysts. Both the bicyclic intermediates **Ab-6** and **Abi-6** have been located 9.5 and 10.0 kcal mol^{-1} below **Ab-3** and **Abi-3**, respectively. However, any attempt to find a transition state connecting **Ab/Abi-4** to **Ab/Abi-6** failed. In this case, we first considered that the activation energy could be negligible and the step considered barrierless, but since no transition state connecting **Ab/Abi-6** to **Ab/Abi-7** converged, we excluded the mechanistic path **1**→**2**→**3**→**6**→**7**→**4**→**5**→**1** (Path 2);[35] it is worth noting that a mechanism analogous to Path 2 is operative when the acetylene cyclotrimerization is catalyzed by [CpRuCl][32] or when CpRh is employed in the co–cyclotrimerization of acetylene and acetonitrile to 2-methylpyridine.[6]

Finally, we explored the possibility of direct insertion of the coordinated acetylene into the Rh–Cα bond, postulated by Schore,[30] that is, **1**→**2**→**3**→**7**→**4**→**5**→**1** (Path 3). The product, that is, the seven-membered rhodacyle converged 40.1 and 35.8 kcal mol^{-1} below **Ab-3** and **Abi-3**, respectively. The corresponding activation energies of this step of the AbRh- and AbiRh-catalyzed processes amount to 9.8 and 7.6 kcal mol^{-1}, respectively. Subsequently the intermediates **7** must undergo reductive elimination to form **4**. This step has a barrier of 17.8 kcal mol^{-1} in the case of the **Ab-7**→**Ab-4** reaction and 16.8 kcal mol^{-1} in the case of **Abi-7**→**Abi-4**. These values are higher than the corresponding energies required to form the five-membered rhodacyle at the beginning and thus the reductive elimination rather than the oxidative coupling becomes the TOF-determining step along Path 3.

In Figure 6, the energetics of the analogous mechanistic path for CpRh catalyzed acetylene cyclotrimerization has been taken from reference [6]. Also in this case the reductive elimination was found by some of us to be the TOF-determining step and its activation energy is higher than that computed for the heteroaromatic catalysts. In order to quantify the performance of AbRh, AbiRh, and CpRh catalysts in the hypothesis of Path 3, the relative TOFs have been computed and are reported in Table 1. This trend of catalytic efficiency can be established AbiRh > AbRh > CpRh. For the heteroaromatic catalysts, the activation energies of the oxidative coupling **1**→**2** are not much lower than the activation energy for the reductive elimination and this supports the prediction of Path 3 as an alternative to Path 1; the same is not valid for CpRh catalysis.[6] Activation strain analyses for the reductive elimination step from **Ab-7** via **Ab-TS74** versus that from **Cp-7** via **Cp-TS74** shed light on the origin of the different activation barriers. The results are reported in Table 4. The fragments are a benzene molecule and the LRh moiety (L=Cp, Ab, Abi). Both in the reac-

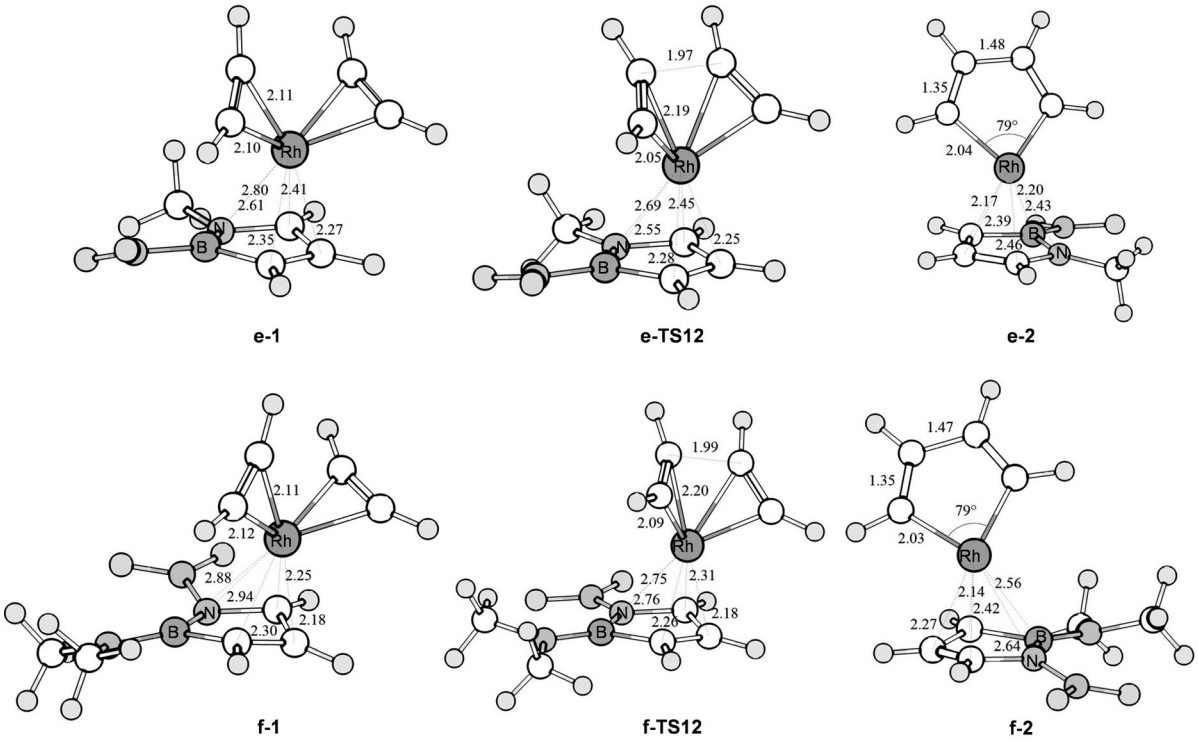

Figure 5. Molecular structures with relevant interatomic distances [Å] and angles [°] of the 1,2-azaborolyl Rh^{I} intermediates **e-1**, **e-2**, **f-1**, **f-2** and transition states **e-TS12**, **f-TS12**.

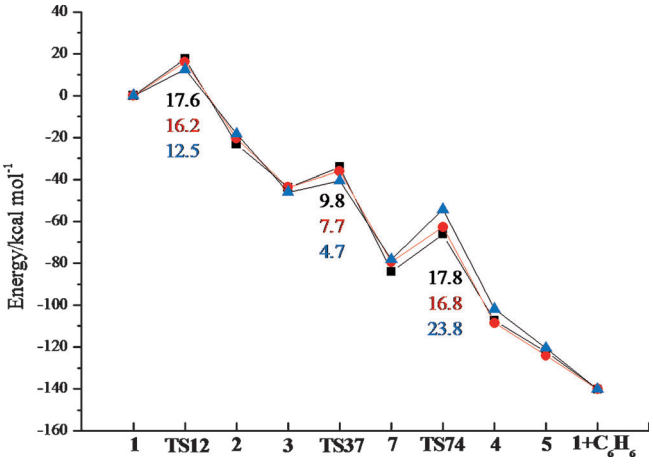

Figure 6. Path 3: energy profile of AbRh (black squares)-, AbiRh (red circles)-, and CpRh (blue triangles)-catalyzed acetylene [2+2+2] cyclotrimerization (see also Scheme 2); activation energies (kcal mol^{-1}) are shown.

tants **7** and in the transition states **TS74** the total strain is less destabilizing according to the trend Abi > Ab > Cp and the interaction less attractive accordingly. $\Delta\Delta E^{\neq}_{strain}$ is comparable for Ab and Abi, but significantly smaller for Cp and, being $\Delta\Delta E^{\neq}_{int}$ much closer in the three cases, this difference explains why in presence of Cp ligand the activation energy for this step is higher. Focusing on the small difference between the activation energies in the case of Ab and Abi,

Table 4. Activation strain analysis of **Cp-7/TS74**, **Ab-7/TS74** and **Abi-7/TS74**; all the values are in [kcal mol^{-1}].

	C_6H_6	$\Delta\Delta E^{\neq}_{strain}$ (L)Rh	Total	$\Delta\Delta E^{\neq}_{int}$	$\Delta E^{\neq}$[a]
Cp-7/Cp-TS74	−50.6	11.6	−39.0	62.8	23.8
Ab-7/Ab-TS74	−51.6	−4.6	−56.2	74.0	17.8
Abi-7/Abi-TS74	−49.5	−5.4	−54.9	71.7	16.8

[a] Activation energy: $\Delta E^{\neq} = \Delta\Delta E^{\neq}_{strain} + \Delta\Delta E^{\neq}_{int}$.

this can be ascribed to a larger $\Delta\Delta E^{\neq}_{int}$ in the former, which is not sufficiently compensated by the negative $\Delta\Delta E^{\neq}_{strain}$. The slippage parameter and the folding angle change from 0.21 Å and 9.7° to 0.39 Å and 11.3° when going from **Ab-7** to **Ab-TS74** and from 0.28 Å and 12.4° to 0.44 Å and 15.1° when going from **Abi-7** to **Abi-TS74**; the corresponding values in the couple **Cp-7**/**Cp-TS74** are 0.00054 Å and 5.9° and 0.077 Å and 6.7°, respectively. As expected, in the heteroaromatic catalysts the slippage increases much more, since the less positive rhodium tends to avoid the sterically crowded [N-B^{-}] region. For **Cp-7** the reductive elimination is more difficult, due to its nearly C_s symmetry, as previously discussed.[6,31] This step is an example of a forbidden disrotatory concerted reaction because a symmetry plane persists from **Cp-7** to **Cp-4**, but the orbital symmetry with respect to this plane is not preserved upon C–C bond formation, that is, occupied–empty orbital crossing occurs. Importantly, the lower activation energy computed for AbiRh than for AbRh for step **7**→**4** is accompanied by more slippage in the

former than in the latter. This is consistent with a classic indenyl effect.

Conclusion

AbRh and AbiRh fragments can catalyze the acetylene [2+2+2] cyclotrimerization to benzene with a mechanism analogous to that reported for CpCo, CpRh, and IndRh fragments. No efficiency improvements of the catalytic activity is predicted when these heteroaromatic ligands are employed instead of the parent isoelectronic and isostructural hydrocarbon ones in a classic CpCo-like mechanism (Path 1). This is in agreement with our previous findings that pronounced hapticity variations of the catalytic fragment, as those described for AbRh and AbiRh, disfavor the process.

When the 1,2-azaborolyl ligand is used, different susbtituents at B and N can be introduced to tune the catalytic activity of the fragment. We have observed that the height of the highest barrier of the catalytic cycle decreases in presence of substituents that reduce the metal slippage.

If an alternative path through a heptacyclic intermediate formed by Schore's insertion is postulated (Path 3), AbRh and AbiRh catalysts perform much better than CpRh. In this case, the initial formation of the five-membered metallacyle is not rate- and TOF-determining, but the reductive elimination of the seven-membered rhodacyle is characterized by the highest activation energy. We have not found any evidence of a [CpRuCl]-like mechanism through a bicyclic intermediate (Path 2) at the employed level of theory.

While prompting for more experimental data to discriminate among the different paths, these results can be outlined as follows:

1) Slippage disfavors paths in which the highest activation energy is found for the intramolecular C–C oxidative coupling to form the coordinatively unsaturated metallacycle; we designate this phenomenon reverse indenyl effect.
2) Along an alternative path in which the highest activation energy is found for an intramolecular reductive elimination, the heteroaromatic catalysts are favored. This is not only related to rhodium slippage, but also to the asymmetry of the Ab and Abi ligands; in fact the reductive elimination, which occurs easily also with the low-symmetry [CpRuCl] catalyst, is, in the case of the almost C_s-symmetric **Cp-7**, symmetry forbidden.
3) The highest activation energy of the whole cycle along Path 1 can be modulated with different substituents at boron, while the effect of substituents at nitrogen is less pronounced.
4) Solvent effects are predicted to have only little influence on the energetics, due to the absence of strongly polar chemical species.

Our results suggest that the present heteroaromatic half-metallocene Rh^I catalysts are amenable to application in alkyne [2+2+2] cyclotrimerizations and their performance can be optimized through selected substituents at the heteroatoms, in particular at boron. Another intriguing aspect, which is currently under investigation, is the cyclocotrimerization of different alkynes and nitriles, in which the asymmetry of the heteroaromatic ligands can be an advantage and play an important role in the regioselectivity of the process.

Acknowledgements

The work has been performed under the HPC-EUROPA2 project (project number: 228398) with the support of the European Commission—Capacities Area—Research Infrastructures. We thank the University of Padova (CPDA127392/12) and Netherlands Organization for Scientific Research (NWO-CW and NWO-EW) for financial support. The calculations were carried out on Huygens at SARA (Amsterdam) and on the TC cluster at VU University Amsterdam. Photos for the cover were taken by the authors at The Butterfly House—Fairies Wood in Montegrotto Terme (Italy) (http://www.micromegamondo.com/casadellefarfalle/index.php) and can be published thanks to the kind permission of the museum direction.

[1] a) G. Schmid, M. Schütz, *Organometallics* **1992**, *11*, 1789–1792; b) G. Schmid, M. J. Schütz, *J. Organomet. Chem.* **1995**, *492*, 185–189; c) G. Schmid, *Comprehensive Heterocyclic Chemistry II, Vol. 3* (Ed.: I. Shinkai), Elsevier, Oxford, **1996**, Chapter 3.17; d) G. Schmid, B. Kilanowski, R. Boese, D. Bläser, *Chem. Ber.* **1993**, *126*, 899–906; e) G. Schmid, F. Schmidt, *Chem. Ber.* **1986**, *119*, 1766–1775; f) G. Schmid, D. Kampmann, W. Meyer, R. Boese, P. Paetzold, K. Delpy, *Chem. Ber.* **1985**, *118*, 2418–2428; g) G. Schmid, S. Amirkhalili, U. Höner, D. Kampmann, R. Boese, *Chem. Ber.* **1982**, *115*, 3830–3841; h) G. Schmid, R. Boese, *Z. Naturforsch. B* **1983**, *38*, 485–492; i) G. Schmid, D. Kampmann, U. Höner, D. Blaser, R. Boese, *Chem. Ber.* **1984**, *117*, 1052–1060.
[2] S.-Y. Liu, M. M.-C. Lo, G. C. Fu, *Angew. Chem.* **2002**, *114*, 182–184; *Angew. Chem. Int. Ed.* **2002**, *41*, 174–176.
[3] a) A. J. Ashe III, X. Fang, *Org. Lett.* **2000**, *2*, 2089–2091; b) A. J. Ashe III, X. Fang, J. W. Kampf, *Organometallics* **2001**, *20*, 5413–5418; c) X. Fang, H. Yang, J. W. Kampf, M. M. Banaszak Holl, A. J. Ashe III, *Organometallics* **2006**, *25*, 513–518.
[4] a) S. Saito, Y. Yamamoto, *Chem. Rev.* **2000**, *100*, 2901–2915; b) J. A. Varela, C. Saa, *Chem. Rev.* **2003**, *103*, 3787–3801; c) D. L. J. Broere, E. Ruijter, *Synthesis* **2012**, *44*, 2639–2672; d) Y. Shibata, K. Tanaka, *Synthesis* **2012**, *44*, 3269.
[5] a) P. Cioni, P. Diversi, G. Ingrosso, A. Lucherini, P. Ronca, *J. Mol. Catal.* **1987**, *40*, 337–357; b) P. Diversi, L. Ermini, G. Ingrosso, A. Lucherini, *J. Organomet. Chem.* **1993**, *447*, 291–298; c) K. Abdulla, B. L. Booth, C. Stacey, *J. Organomet. Chem.* **1985**, *293*, 103–114.
[6] L. Orian, J. N. P. Van Stralen, F. M. Bickelhaupt, *Organometallics* **2007**, *26*, 3816–3830.
[7] L. Orian, *Rev. Roum. Chim.* **2007**, *52*, 551–558.
[8] a) L. Orian, P. Ganis, S. Santi, A. Ceccon, *J. Organomet. Chem.* **2005**, *690*, 482–492; b) L. Orian, A. Bisello, S. Santi, A. Ceccon, G. Saielli, *Chem. Eur. J.* **2004**, *10*, 4029–4040; c) S. Santi, L. Orian, A. Bisello, C. Durante, P. Ganis, A. Ceccon, F. Benetollo, L. Crociani, *Chem. Eur. J.* **2007**, *13*, 1955–1968; d) S. Santi, L. Orian, C. Durante, E. S. Bencze, A. Bisello, A. Donoli, A. Ceccon, F. Benetollo, L. Crociani, *Chem. Eur. J.* **2007**, *13*, 7933–7947; e) S. Santi, C. Durante, A. Donoli, A. Bisello, L. Orian, A. Ceccon, L. Crociani, F. Benetollo, *Organometallics* **2009**, *28*, 3319–3326; f) S. Santi, C. Durante, A.

Donoli, A. Bisello, L. Orian, F. Benetollo, P. Ganis, A. Ceccon, *Organometallics* **2010**, *29*, 2046–2053.
[9] M. J. Calhorda, C. C. Romão, L. F. Veiros, *Chem. Eur. J.* **2002**, *8*, 868–875.
[10] a) H. Adams, N. A. Bailey, B. E. Mann, B. F. Taylor, C. White, P. Yavari, *J. Chem. Soc. Dalton Trans.* **1987**, 1947–1951; b) A. K. Kakkar, S. F. Jones, N. J. Taylor, S. Collins, T. B. Marder, *J. Chem. Soc. Chem. Commun.* **1989**, 1454–1456; c) S.-Y. Liu, I. D. Hills, G. C. Fu, *Organometallics* **2002**, *21*, 4323–4325.
[11] In the heteroaromatic complexes, the slippage parameter Δ is calculated replacing the distances Rh−C1a and Rh−C3a with Rh-N and Rh−B respectively.
[12] a) P. Hohenberg, W. Kohn, *Phys. Rev.* **1964**, *136*, B864–B871; b) W. Kohn, L. J. Sham, *Phys. Rev.* **1965**, *140*, A1133; c) R. G. Parr, W. Yang *Density-Functional Theory of Atoms and Molecules*; Oxford University Press, New York, **1989**.
[13] E. J. Baerends, D. E. Ellis, P. Ros, *Chem. Phys.* **1973**, *2*, 41–51.
[14] a) G. te Velde, F. M. Bickelhaupt, E. J. Baerends, C. Fonseca Guerra, S. J. A. van Gisbergen, J. G. Snijders, T. Ziegler, *J. Comput. Chem.* **2001**, *22*, 931–967; b) Computer code ADF2007 and ADF2012.01: E. J. Baerends, et al. (SCM, Theoretical Chemistry, Vrije Universiteit, Amsterdam, The Netherlands, **2007–2012**).
[15] E. van Lenthe, E. J. Baerends, J. G. Snijders, *J. Chem. Phys.* **1994**, *101*, 9783–9792.
[16] a) A. D. Becke, *Phys. Rev. A* **1988**, *38*, 3098–3100; b) C. Lee, W. Yang, R. G. Parr, *Phys. Rev. B* **1988**, *37*, 785–789.
[17] a) W.-J. van Zeist, F. M. Bickelhaupt, *Org. Biomol. Chem.* **2010**, *8*, 3118–3127; b) G. Th. de Jong, F. M. Bickelhaupt, *ChemPhysChem* **2007**, *8*, 1170–1181; c) F. M. Bickelhaupt, *J. Comput. Chem.* **1999**, *20*, 114–128; d) F. M. Bickelhaupt, E. J. Baerends, in *Reviews in Computational Chemistry, Vol. 15* (Eds.: K. B. Lipkowitz, D. B. Boyd) Wiley-VCH, Weinheim, **2000**, pp. 1–86.
[18] a) G. Th. de Jong, M. Solà, L. Visscher, F. M. Bickelhaupt, *J. Chem. Phys.* **2004**, *121*, 9982–9992; b) G. Th. de Jong, D. P. Geerke, A. Diefenbach, F. M. Bickelhaupt, *Chem. Phys.* **2005**, *313*, 261–270.
[19] G. Th. de Jong, D. P. Geerke, A. Diefenbach, M. Solà, F. M. Bickelhaupt, *J. Comput. Chem.* **2005**, *26*, 1006–1020.
[20] G. Th. de Jong, F. M. Bickelhaupt, *J. Phys. Chem. A* **2005**, *109*, 9685–9699.
[21] G. Th. de Jong, F. M. Bickelhaupt, *J. Chem. Theory Comput.* **2006**, *2*, 322–335.
[22] L. Orian, W. J. van Zeist, F. M. Bickelhaupt, *Organometallics* **2008**, *27*, 4028–4030.
[23] a) A. Klamt, G. Schüürmann, *J. Chem. Soc. Perkin Trans. 2* **1993**, 799–805; b) A. Klamt, *J. Phys. Chem.* **1995**, *99*, 2224–2235.
[24] N. L. Allinger, X. Zhou, J. Bergsma, *J. Mol. Struct. THEOCHEM* **1994**, *312*, 69–83.
[25] R. S. Bon, B. van Vliet, N. E. Sprenkels, R. F. Schmitz, F. J. J. de Kanter, Chr. V. Stevens, M. Swart, F. M. Bickelhaupt, M. B. Groen, R. V. A. Orru, *J. Org. Chem.* **2005**, *70*, 3542–3553.
[26] I. Fernández, F. M. Bickelhaupt, F. P. Cossio, *Chem. Eur. J.* **2012**, *18*, 12395–12403.
[27] C. Amatore, A. Jutand, *J. Organomet. Chem.* **1999**, *576*, 254–278.
[28] a) S. Kozuch, S. Shaik, *Acc. Chem. Res.* **2011**, *44*, 101–110; b) S. Kozuch, S. Shaik, *J. Am. Chem. Soc.* **2006**, *128*, 3355–3356; c) S. Kozuch, S. Shaik, *J. Phys. Chem. A* **2008**, *112*, 6032–6041; d) A. Uhe, S. Kozuch, S. Shaik, *J. Comput. Chem.* **2011**, *32*, 978–985.
[29] L. Orian, M. Swart, F. M. Bickelhaupt, unpublished results.
[30] N. E. Schore, *Chem. Rev.* **1988**, *88*, 1081–1119.
[31] J. H. Hardesty, J. B. Koerner, T. A. Albright, G.-Y. Lee, *J. Am. Chem. Soc.* **1999**, *121*, 6055–6067.
[32] a) K. Kirchner, M. J. Calhorda, R. Schmid, L. F. Veiros, *J. Am. Chem. Soc.* **2003**, *125*, 11721–11729; b) M. J. Calhorda, P. J. Costa, K. Kirchner, *Inorg. Chim. Acta* **2011**, *374*, 24–35; c) Y. Yamamoto, T. Arakawa, R. Ogawa, K. Itoh, *J. Am. Chem. Soc.* **2003**, *125*, 12143–12160; d) Y. Yamamoto, K. Kinpara, T. Saigoku, H. Takagishi, S. Okuda, H. Nishiyama, K. Itoh, *J. Am. Chem. Soc.* **2005**, *127*, 605–613; e) Y. Yamamoto, K. Kinpara, R. Ogawa, H. Nishiyama, K. Itoh, *Chem. Eur. J.* **2006**, *12*, 5618–5631.
[33] M. E. Rerek, L. N. Ji, F. Basolo, *J. Chem. Soc. Chem. Commun.* **1983**, 1208.
[34] In 1995, Sweigart and co-workers reported on an "inverse indenyl effect" observed in dissociative ligand substitutions in 19-electron complexes $[(\eta^5\text{-Cp})Fe(CO)_3]$ and $[(\eta^5\text{-Ind})Fe(CO)_3]$. Their inverse indenyl effect has a fundamentally different appearance and nature than our reverse indenyl effect. In the reaction studied by Sweigart et al., the reactivity is reduced in the case that no slippage change from η^5 to η^3 occurs, consistent with what is commonly termed indenyl effect. However, in their case, this absence of slippage and reduced reactivity occurs exactly for the indenyl complex. To avoid overlap in terminology with the effect revealed by us (i.e., reduced reactivity in the case of more slippage of the indenyl ligand) we propose here the slightly different designation of a "reverse indenyl effect". K. A. Pevear, M. M. Banaszak Holl, G. B. Carpenter, A. L. Rieger, P. H. Rieger, D. A. Sweigart, *Organometallics* **1995**, *14*, 512–523.
[35] A careful search of the transition states **Ab/Abi-TS67** was carried out starting from LT profiles along the reaction coordinate defined as the distance between Rh and the γ-C of the heptacyclic ring. In the case of **Ab-TS67**, the energy profile does not converge in all points (maximum displacement of 0.1 Å and 100 optimization cycles for each step); the search for a transition state using the geometry of the maximum leads to a structure characterised by a single imaginary frequency, which is not the transition state of interest, but closely resembles the transition state of the interconversion between the two possible bicycles. This transition state lies 19.7 kcal mol^{-1} above **6**. In the case of AbiRh, the linear transit is not a bell-shaped curve, but the energy initially smoothly decreases, then suddenly increases to the maximum and finally drops to the lower value of the product and any attempt of transition state optimization lead either to the reactant or to the product.

Received: May 23, 2013
Published online: September 3, 2013

